

Direct Observation of Individual Hydrogen Atoms at Trapping Sites in a Ferritic Steel

Y-S. Chen¹, D. Haley^{1*}, S. S. A. Gerstl², A. J. London¹,
F. Sweeney³, R. A. Wepf^{2,4}, W. M. Rainforth³,
P. A. J. Bagot¹, M. P. Moody¹

¹Department of Materials, Oxford University,
16 Parks Road, Oxford, OX1 3PH, UK,

²Scientific Center for Optical and Electron Microscopy, ETH Zürich
Auguste-Piccard-Hof 1, 8093, Zürich, Switzerland

³Department of Materials Science and Engineering, Sheffield University
Western Bank, Sheffield, S10 2TN, UK

⁴Centre for Microscopy and Microanalysis, Faculty of Science, University of Queensland
Brisbane QLD 4072, Australia

*E-mail: daniel.haley@materials.ox.ac.uk.

One Sentence Summary

The three-dimensional distribution of individual hydrogen atoms within a complex steel microstructure is characterized using isotopic doping and cryogenic-transfer atom probe tomography.

Abstract

The design of atomic-scale microstructural traps to limit the diffusion of hydrogen is one key strategy in the development of hydrogen-

embrittlement resistant materials. In the case of bearing steels, an effective trapping mechanism may be the incorporation of finely dispersed V-Mo-Nb-carbides in a ferrite matrix. First, we charged a ferritic steel with deuterium by electrolytic loading to achieve a high hydrogen concentration. We then immobilized it in the microstructure with a cryogenic transfer protocol prior to Atom Probe Tomography (APT) analysis. Using APT we show trapping of hydrogen within the core of these carbides with quantitative composition profiles. Furthermore, using this method, the experiment can be feasibly replicated in any APT equipped laboratory using a simple cold-chain.

1 Article

Hydrogen embrittlement, whereby the presence of hydrogen within a material's microstructure causes a severe loss in ductility, can lead to catastrophic and unpredictable failure of structural components in service (1) (2). This is critical in many applications, as hydrogen is a near-ubiquitous element, and can enter either the material at the time of manufacture or later during use. Hydrogen embrittlement affects many applications, such as fasteners in aircraft and bolts used in the construction of bridges. As such, it is a serious concern in many marine and civil engineering applications (3) (4). Hydrogen embrittlement is particularly important in the area of advanced high strength steels for the automotive sector, where the steel strength now exceeds 1 GPa, resulting in a material much more susceptible to hydrogen embrittlement. Such hydrogen embrittlement concerns can lead to the selection of higher cost or alternatively, reduced performance alloys - particularly in terms of tensile strength.

Mitigating hydrogen embrittlement usually involves either annealing to remove hydrogen that has been introduced during manufacture, or applying barrier coatings to minimize further ingress of hydrogen from external sources (5). However, a third option is to imbue materials with an intrinsic resilience. Our poor understanding of how hydrogen interacts with microstructure at the atomic scale limits this option, despite general agreement that the diffusion of hydrogen within a microstructure is a key factor for hydrogen embrittlement (6). More generally, despite the clearly serious nature of hydrogen embrittlement, and a large body of macroscopic experimental and simulation research, there exists little in the way of direct observation of hydrogen within these materials. This is due to the experimental difficulty of directly observing hydrogen within technologically relevant microstructures (7). This makes it challenging to engineer microstructures that will mitigate the effect.

Practically, after low-to-moderate heat-treatment schedules to remove hydrogen from within parts after manufacture (8), protective barriers can reduce further ingress of hydrogen from environmental sources during service. However, protective barriers can fail in the presence of abrasive or degrading environments, providing a pathway for hydrogen and embrittlement (9). The incorporation of finely dispersed nano-scaled carbides (10) (11) (12), such as ~ 10 nm VC carbides (13) (14) offer a suite of options for intrinsically resistant steels. The carbides act as “traps” to retain hydrogen that might otherwise diffuse through the microstructure and promote embrittlement. The traps may either operate to limit apparent diffusion rates (15) in a reversible manner, and/or they may sequester hydrogen within their own microstructures (14). Again, little direct experimental information exists on the interaction of hydrogen with such precipitates. Whilst some theoretical predictions do exist, they are limited to cases that are straightforward to simulate, e.g. via DFT (16). The uncertainty in the effectiveness of hydrogen trapping by these microstructures in turn

leads to great uncertainty in microstructural design.

Hydrogen trapping in bulk samples is studied by several methods, such as Small-Angle Neutron Scattering (17), Thermal Desorption Spectroscopy (15) (18), and Energy Recoil Detection (19). These methods provide only bulk-averaged information on microstructural interaction, and the direct interpretation from these signals is difficult. Secondary Ion Mass Spectroscopy can directly image hydrogen (20) (21) (22) (23), but it cannot measure the precise location of hydrogen atoms, which limits applicability. At smaller scales, Transmission Electron Microscopy (TEM) can detect hydrogen in very specific cases, such as hydrogen imaging on graphene (24), or hydrogen induced phase changes (25). Such TEM methods fail to provide robust results when facing more complex systems, such as hydrogen within an iron carbide (26), where projection and diffraction effects may dominate.

However, one possible alternative technique is Atom Probe Tomography (APT). This method is a three dimensional microscopy technique with near atomic resolution (27), that can resolve the chemical identities of individual atoms within a target material, even for light elements (28). Unfortunately, while in theory APT can resolve hydrogen without any instrumental modification, naturally occurring hydrogen is present as a major element in most analyses. Hydrogen in these cases is primarily a contaminant from the high vacuum chamber of these systems (29) (30). This means interpretation of the ^1H signal is severely limited by the ambiguity of its origins, and for the most part it is simply ignored in typical analyses.

To address this limitation, several researchers have used deuterium (^2H) to distinguish environmentally derived hydrogen from that deliberately introduced for analysis. Deuterium's natural scarcity (1.2×10^{-4} fraction of natural hydrogen), guarantees that nearly all deuterium detected originates from the sample's microstructure. However other chal-

lenges remain that limit quantitative spatial information on the hydrogen distribution in engineering microstructures at the atomic scale.

To circumvent the remaining challenges for high quality measurements of the spatial distribution of hydrogen, we combine two approaches to APT hydrogen charging experiments, electrolytic charging (31) and cryogenic transfer (32). By utilizing the two approaches in concert, we provide a quantitative measure of the 3D hydrogen content within a proposed VMoNbC containing steel.

In hydride forming systems, APT can image deuterium introduced to the material through gaseous charging (33). However, the low solubility of deuterium within both ferrite and austenite (34) means limited data for deuterium in steel is available. A notable exception to this is the work of Takahashi *et al*, wherein deuterium was qualitatively shown to correlate to the positions of vanadium and titanium carbides (32) (35), through a combination of annealing, gaseous charging and rapid quenching. Recently, work has been undertaken using a D₂O charging approach. Theoretically, a D₂O charging approach should achieve a higher deuterium content (31). In recent work using this approach no spatial data was shown for steel samples primarily due to diffusion losses.

Examining a VC containing ferritic steel (Fig. 1), we used a high fugacity electrolytic method to charge hydrogen to high concentrations, in conjunction with a cryogenic transfer, to suppress loss of hydrogen via diffusion during transfer to the atom probe. We utilized an existing cryo-transfer system, designed to also accommodate biological or liquid specimen transfers (36) with similar experimental protocols. This approach provides a complete and stringent cold-chain, post hydrogen charging, from laboratory bench-top to the atom probe ultra-high vacuum chamber (Fig. S1). The procedure requires a cold-chain, however a considerably less advanced system than used here may also prove effective in hydrogen detection.

To perform the deuterium charging, there are several straightforward requirements. Firstly, a specimen in the needle-geometry required for APT is prepared from the steel sample using standard electropolishing techniques (28). The specimen is then subjected to a short analysis in the atom probe system. The result of this step is that post-experiment the field evaporation process that underpins APT effectively provides an atomically clean surface (37). The electrolytic charging process is then conducted in a charging solution, consisting of a deuterated electrolyte (NaOD, 0.1 M) in heavy water (D_2O). The in-vacuum cold-chain is incorporated into the process to suppress hydrogen diffusion, whilst entirely avoiding ice formation. The full details of the experimental component of this approach are given in the supplementary methods section (38).

We electrolytically deuterated a sample of ferritic steel and transferred at approximately 100 K for an atom probe experiment (Fig. 2). The highlighted deuterium atoms (red) correspond to the mass-to-charge peak observed at 2 Da. To verify that the atoms shown are actually deuterium, and not H_2 , an additional control sample was charged using light water (H_2O) charged and analyzed in the exact same manner, wherein unlike the heavy-water charged dataset, no peak at 2 Da was observed (Fig. S3).

The positions of the deuterium atoms show a strong correlation to the proposed vanadium carbide trapping sites in this material, consistent with earlier work (32). Visual inspection of the dataset does not allow for identification of the exact location of the hydrogen, as either within each individual carbide, or at the carbide-matrix interface. This is partly due to the limited number of atoms involved. Indeed, an ongoing debate exists about whether the hydrogen is at the surface (39), or penetrates into the carbide itself (17). Previous qualitative APT analysis suggests that this may be a surface effect (32), but no quantitative data confirms this result. In order to maximize the hydrogen trapping potential, the location of the hydrogen relative to the trapping inclusions

has considerable ramifications.

To further investigate the spatial location of hydrogen, relative to that of the carbide, we analyzed our data using an advanced statistical procedure for combining information from multiple precipitates within a single dataset (40). In this work we selected all the carbides incorporating more than 100 total ions, then computed the radius of gyration normal to z for the particles (r_g). We collected composition profiles from each particle (and surrounding matrix) along the Z-axis of the particle (four times the particles full Z bounds), using a square aperture of length $2r_g$. We normalized the profile's Z distance to 0-1 (0 \rightarrow start of particle, 1 \rightarrow end of particle along Z). Finally we accumulated the profiles to form a single combined composition profile (Fig. 3), where we observe that the deuterium is restricted to the interior of the carbide, wherein it reaches a maxima before decaying. If hydrogen was restricted to the interfacial region at the surface, we would have found a U-shaped profile, which is clearly not the case in the data presented here.

These results are consistent with neutron scattering results, such as given by Malard (17), who undertook charging using a 0.1 M NaOH solution. In their work, they observed a change in the neutron scattering data after charging with hydrogen in a VC containing steel with hydrogen. However, this is in contrast with the neutron scattering work of Ohnuma (39) on a steel containing NbC precipitates, where it was suggested that hydrogen is present at the interface. Malard estimated that at most 5 ppm wt% of hydrogen was contained within the precipitates, which given their volume fractions corresponded to 10at% H contained in the precipitate. In our work, we find a peak deuterium concentration of 0.6at%, and an average concentration of $0.01\% \pm 0.0025\%$ (Counting error, 2-std dev). This however may be under-estimated from the as-charged condition, due to diffusion during the transfer from the charging unit to the cryogenic apparatus.

These results are critical to further understanding the role of hydrogen within steel

microstructures, however the technique is not limited to these materials. Other trapping sites, such as grain and phase boundaries may prove of significant in the design of hydrogen-resistant materials, and this approach has the potential to provide new insight. Furthermore, the method may prove useful elsewhere - systems that may be of interest include nickel superalloy materials, titanium alloys, and austenitic steels, where hydrogen may play an important role in determining macroscopic mechanical properties. We believe that the approach demonstrated here, using liquid charging and cryogenic transfer, is a valuable tool in understanding hydrogen embrittlement from a microstructural perspective.

References and Notes

1. I. M. Robertson, *et al.*, *Metallurgical and Materials Transactions B* **46**, 1085 (2015).
2. V. Reitenbach, L. Ganzer, D. Albrecht, B. Hagemann, *Environmental Earth Sciences* **73**, 69276937 (2015).
3. I. M. Bernstein, *Materials Science and Engineering* **6**, 1 (1969).
4. A. Kuduzović, *et al.*, *Materials Science and Engineering: A* **590**, 66 (2014).
5. H. K. D. H. Bhadeshia, *ISIJ International* **56**, 24 (2016).
6. C. San Marchi, *et al.*, *International Journal of Hydrogen Energy* **In Press** (2016).
7. S. Evers, S. Ceylan, M. Rohwerder, *Science and Technology of Advanced Materials* **14**, 014201 (2013).
8. Astm b850-98(2015), standard guide for post-coating treatments of steel for reducing the risk of hydrogen embrittlement, *Tech. rep.*, West Conshohocken, PA (2015).

9. G. Chalafris, M. J. Robinson, *Corrosion Engineering, Science and Technology* **40**, 28 (2005).
10. T. Kushida, *et al.*, *Tetsu-to-Hagane(Journal of the Iron and Steel Institute of Japan)(Japan)* **82**, 297 (1996).
11. G. Spencer, D. Duquette, The role of vanadium carbide traps in reducing the hydrogen embrittlement susceptibility of high strength alloy steels., *Tech. Rep. ARCCB-TR-98016*, DTIC Document (1998).
12. H. Asahi, D. Hirakami, S. Yamasaki, *ISIJ international* **43**, 527 (2003).
13. K. Kawakami, T. Matsumiya, *ISIJ international* **52**, 1693 (2012).
14. S. Yamasaki, H. Bhadeshia, *Proceedings of the Royal Society A: Mathematical, Physical and Engineering Sciences* **462**, 23152330 (2006).
15. W. Choo, J. Y. Lee, *Journal of Materials Science* **17**, 1930 (1982).
16. T. Hickel, *et al.*, *JOM* **66**, 1399 (2014).
17. B. Malard, *et al.*, *Materials Science and Engineering: A* **536**, 110 (2012).
18. F. Wei, K. Tsuzaki, *Metallurgical and Materials Transactions A* **37**, 331 (2006).
19. K. Fukutani, *Current opinion in solid state and materials science* **6**, 153 (2002).
20. P. Kesten, *et al.*, *Journal of Alloys and Compounds* **330**, 225 (2002).
21. K.-i. Takai, Y. Chiba, K. Noguchi, A. Nozue, *Metallurgical and Materials Transactions A* **33**, 2659 (2002).
22. A. Nishimoto, *et al.*, *ISIJ International* **55**, 335 (2015).

23. Z. Tarzimoghadam, *et al.*, *Acta Materialia* **109**, 69 (2016).
24. J. C. Meyer, C. O. Girit, M. Crommie, A. Zettl, *Nature* **454**, 319 (2008).
25. R. Ishikawa, *et al.*, *Nature materials* **10**, 278 (2011).
26. K. Tatsumi, S. Muto, T. Yoshida, *Journal of applied physics* **101**, 023523 (2007).
27. I. Arslan, E. Marquis, M. Homer, M. A. Hekmaty, N. Bartelt, *Ultramicroscopy* **108**, 1579 (2008).
28. M. K. Miller, A. Cerezo, M. Hetherington, G. D. Smith, *Atom Probe Field Ion Microscopy* (Clarendon Press, 1996).
29. Y. Kunimune, *et al.*, *AIP Advances* **6**, 045121 (2016).
30. G. Sundell, M. Thuvander, H.-O. Andrén, *Ultramicroscopy* **132**, 285 (2013).
31. D. Haley, S. Merzlikin, P. Choi, D. Raabe, *International Journal of Hydrogen Energy* **39**, 1222112229 (2014).
32. J. Takahashi, K. Kawakami, T. Tarui, *Scripta Materialia* **67**, 213 (2012).
33. R. Gemma, T. Al-Kassab, R. Kirchheim, A. Pundt, *Scripta Materialia* **67**, 903 (2012).
34. R. A. J. Karnesky, N. Bartel, D. Huang, N. Teslich, M. Kumar, Imaging and quantification of hydrogen isotope trapping, *Tech. Rep. SAND2012-8539*, Sandia National Laboratories, Albuquerque, New Mexico 87185 and Livermore, California 94550 (2012).
35. J. Takahashi, K. Kawakami, Y. Kobayashi, T. Tarui, *Scripta Materialia* **63**, 261 (2010).

36. S. S. A. Gerstl, R. Wepf, *Microscopy and Microanalysis* **21**, 517 (2015).
37. T. Tsong, *Atom-Probe Field Ion Microscopy: Field Ion Emission, and Surfaces and Interfaces at Atomic Resolution* (Cambridge University Press, 2005).
38. Materials and Methods are available as Supplementary materials on Science Online.
39. M. Ohnuma, J.-i. Suzuki, F.-G. Wei, K. Tsuzaki, *Scripta Materialia* **58**, 142 (2008).
40. A. London, *et al.*, *Ultramicroscopy* **159**, 360 (2015).
41. R. Marceau, P. Choi, D. Raabe, *Ultramicroscopy* **132**, 239247 (2013).
42. M. Thuvander, *et al.*, *Ultramicroscopy* **111**, 604608 (2011).

Acknowledgments

1. Data can be accessed online, via the Oxford Research Archive : <https://ora.ox.ac.uk/objects/uu>
2. The authors would like to acknowledge the support of the EPSRC HeMs project, EP/L014742/1, and the platform grant EP/M022803/1.
3. Y-S. Chen would like to acknowledge support from the Ministry of Education of Taiwan.
4. S. S. A. Gerstl and R.Wepf would like to acknowledge support from the Swiss National Science Foundation (206021_128732/1)

Contributions

Y-S. Chen conducted the charging experiments, prepared samples, optimized the charging process and undertook the data collection and analysis. D. Haley designed the charging

unit and original experimental procedure, aided with the charging experiments and data analysis, and wrote the manuscript. S.S.A. Gerstl and R. Wepf designed, constructed and optimized the cryogenic transfer system. S. S. A. Gerstl additionally designed the cryo experimental procedure, and aided in conducting the charged experiments with cryo-transfer and acquiring the data. A.J. London developed and applied the super-imposed particle analysis procedure. W. M. Rainforth provided the nanoprecipitated carbide steel, and F. Sweeney undertook TEM observations. M.P. Moody, P.A.J.Bagot and W. M. Rainforth are principal investigators on the HeMs project for this work package.

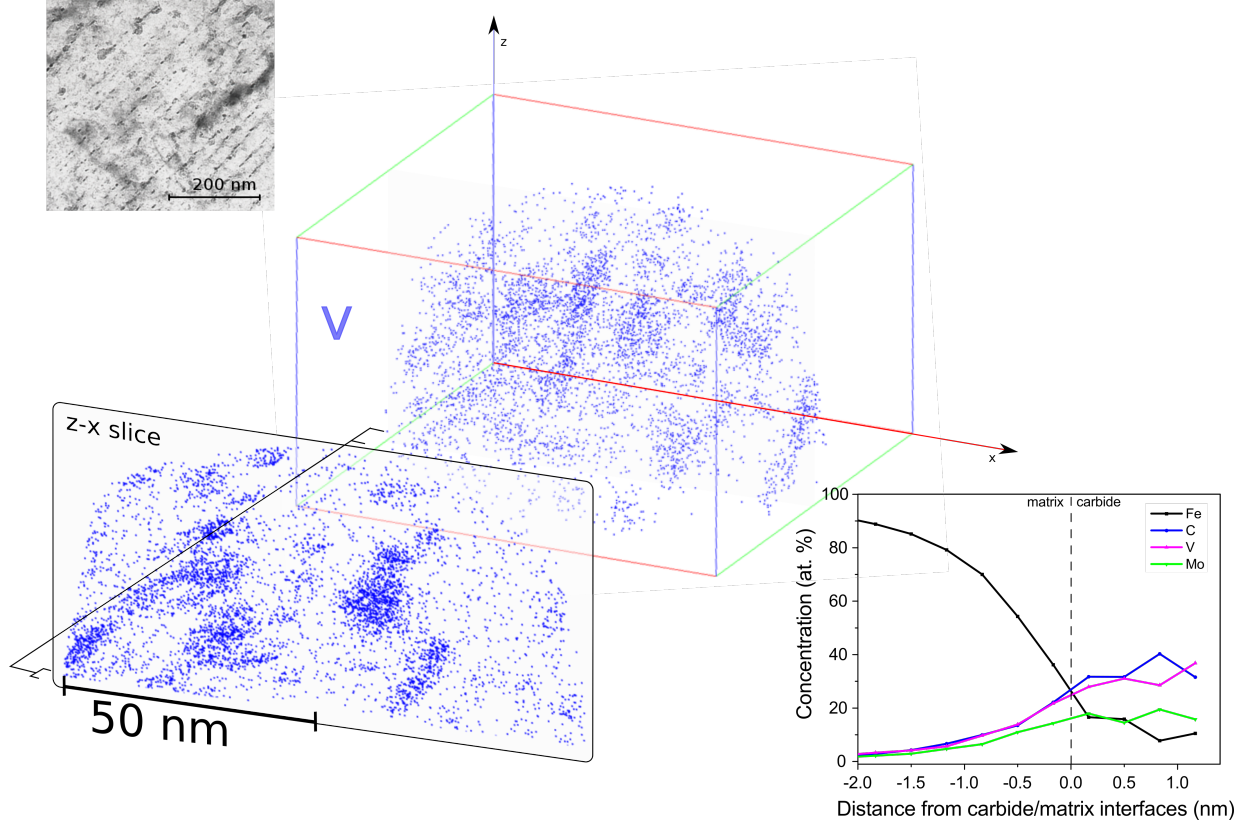


Figure 1: **As-received ferritic VC steel.** 3D map of V in VC Fe-0.096C-1.6Mn-0.026Si-0.51Mo-0.25V-0.05Al-0.056Nb (wt. %) ferritic steel, as obtained via Atom Probe Tomography. Slice is 10 nm in thickness, to highlight the V-containing carbides. Inset bright field TEM image for reference, showing “tracks” of carbides. Composition “proximity histogram”, computed from a 25% V+Mo isosurface shows segregation of V, Mo and C into the carbide phase. Segregated Nb not shown in profile for visual clarity.

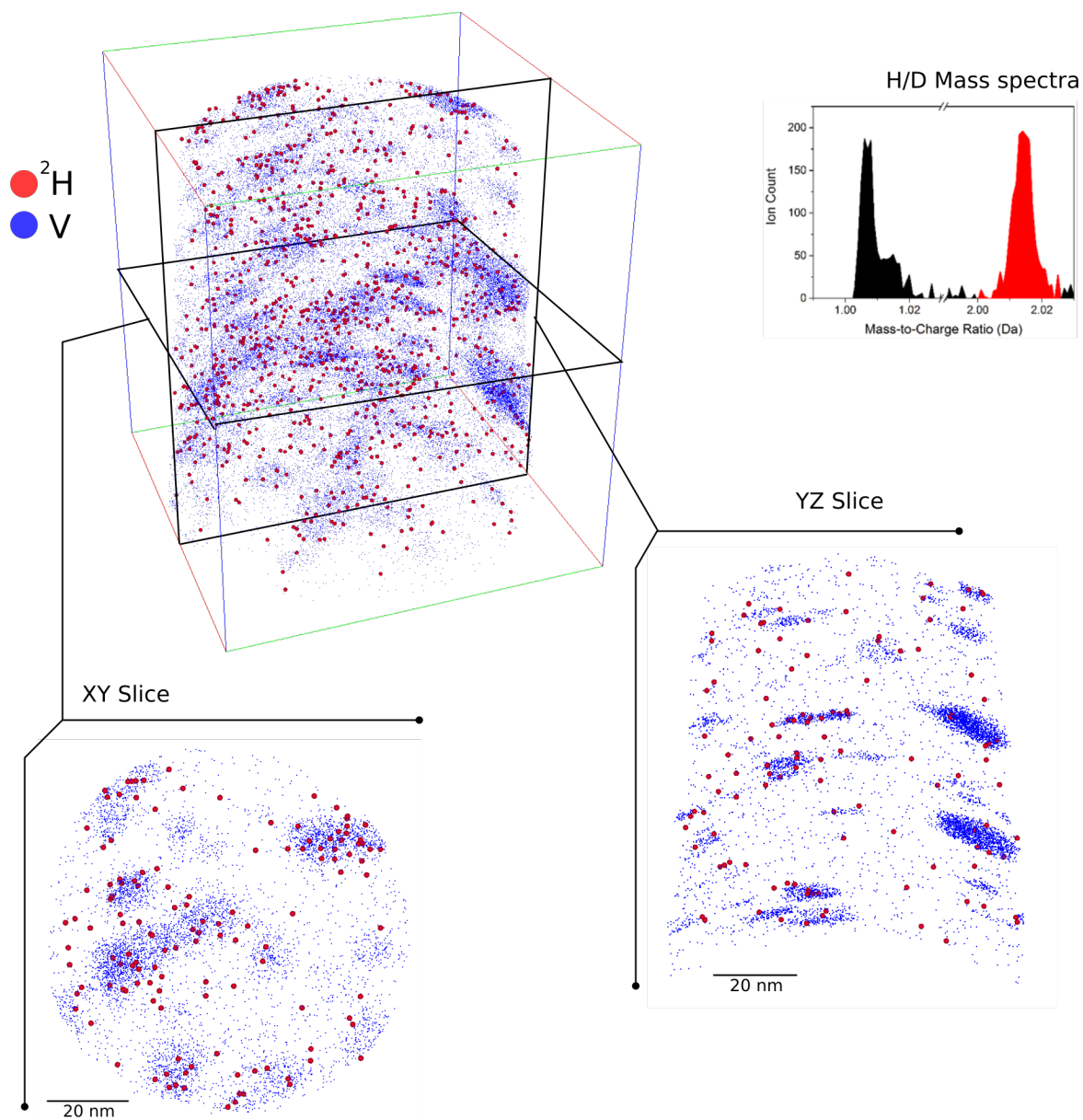


Figure 2: **Introduced deuterium co-located with vanadium carbides.** 3D view of deuterated ferritic steel, showing individual carbides. As can be seen from the top-down and side- slices, deuterium atoms (^2H) are correlated to the carbide positions.

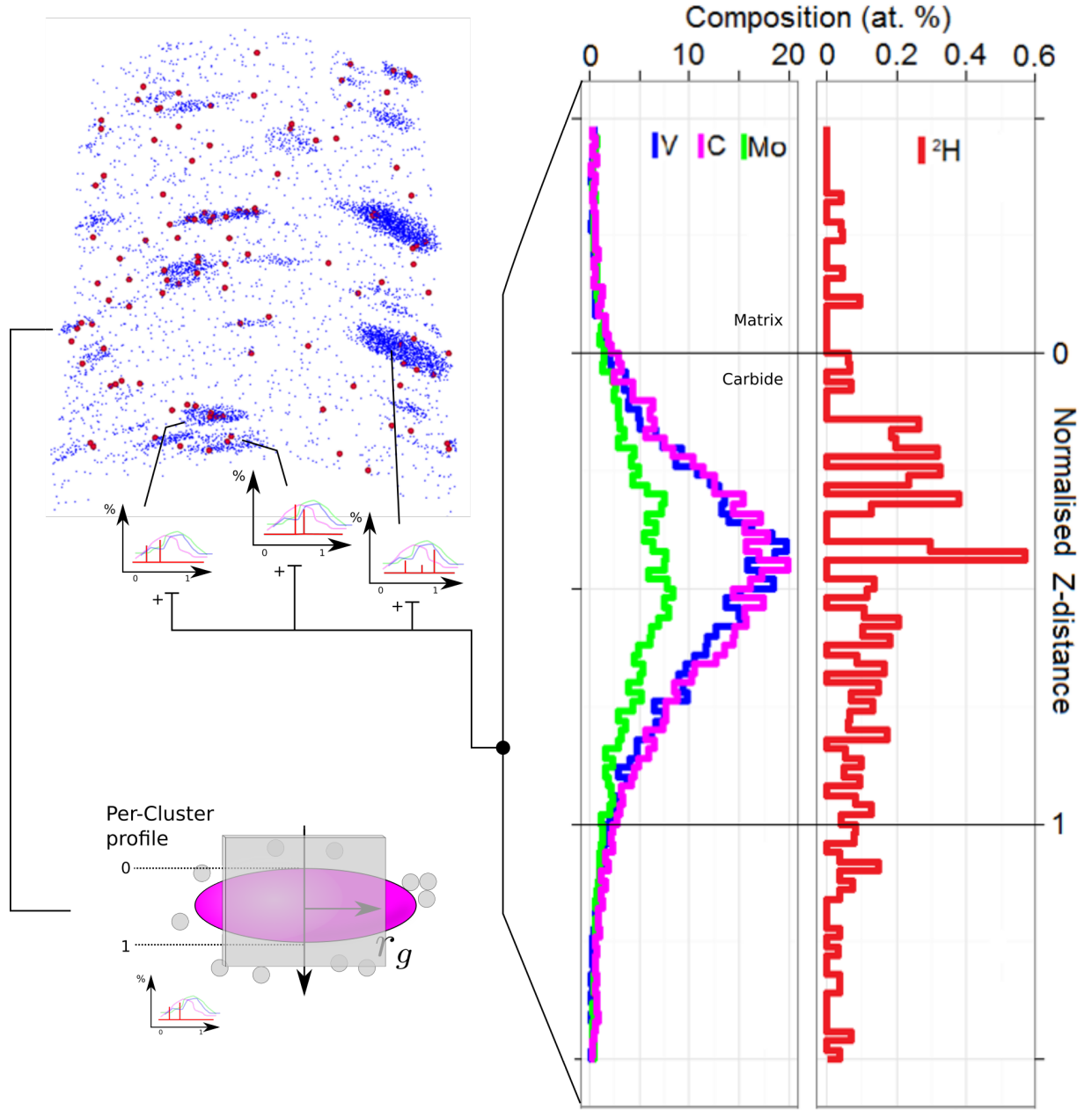


Figure 3: **Combined analysis of deuterium charged carbides.** Superimposed profile of carbides, generated by normalizing and combining multiple individual profiles from each VC (>100 atoms). Resultant profile shows deuterium within the carbide, at ≈ 0.5 at% concentration. Atom map shows ≈ 10 nm slice through dataset

Supplementary Materials

1. Materials and Methods
2. Figs. S1 to S3
3. References (40,41)

Materials and Methods

A ferritic steel of nominal composition of Fe-0.096C-1.6Mn-0.026Si-0.51Mo-0.25V-0.05Al-0.056Nb (wt%) with a very fine dispersion of nanoscale carbides within the ferritic matrix was supplied by Tata Steel Europe. Fig. 1 shows some standard TEM and APT characterization of the steel in its as-received state. In this APT analysis the composition of the material was determined to be Fe-0.071C-1.34Mn-0.029Si-0.51Mo-0.24V-0.053Al-0.056Nb (wt%), which is in good agreement with the nominal composition. Additionally, from the APT analysis the carbide density was measured to be on the order of $10^5 \mu\text{m}^{-3}$, with a volume fraction of 2% - the primary composition of the carbides was found to be 4:3.7:2:0.2 C:V:Mo:Nb (V isosurface >25 at.%). Due to small deviations in carbon measurements typical in APT (41) (42), we do not specifically assign this to be either VC or V_4C_3 . Of note, upon inspection of the mass-to-charge spectrum from the APT analysis of the as-received material, whilst a strong hydrogen signal exists at a mass-to-charge of 1 Da, notably there exists no identifiable peak at 2 Da (Fig. S3).

APT samples were cut to approximately $1 \times 1 \times 15$ mm sections, and electropolished using standard solutions (28). APT data was acquired using voltage mode at 60 K, 200 kHz pulse frequency, a 0.4 % evaporation rate, and 15 % pulse fraction. Samples were initially run in Oxford on a LEAP 3000HR system, to ensure needles were sharp, and to confirm bulk composition in the as-received state. Subsequently, samples were transported

under rough vacuum to ETH Zürich, and loaded into the cryo-transfer equipped atom probe (LEAP 4000-XHR), wherein a reference spectrum was obtained prior to charging which also re-cleaned the sample apex.

Charging was conducted using a 0.1 M NaOH in H₂O (H as either ¹H, or ²H for protiated or deuterated experiments respectively), at 2.2 V for 30 s, using an apparatus similar to that in previous works (31). A Keithley 487 pico-ammeter/voltage source was used for power supply and current measurement, and a small camera was used to ensure that samples were inserted into the solution. Samples were immersed well below the analysis depth as shown in Fig. S2, ensuring that only the steel sample was in contact with the solution. Small bubbles were visible during the charging process.

As shown in Fig. S1, the sample was loaded into a vacuum transfer shuttle (Leica VCT-100) at room temperature and pressure, and then transferred into a freeze-etching unit (Baltec BAF) to both evacuate the chamber (10⁻⁶ Pa) and to provide cooling. The stage temperature of the BAF was set to 100 K. Once the temperature reached steady state (\approx 20 min), the sample was removed from the freeze etcher and returned to the thermally isolated vacuum transfer shuttle. The shuttle was then connected to the atom probe, and the sample transferred into a cryo-carousel, which was pre-cooled to ensure cryogenic temperatures were maintained. A cold trap around the docking port (both on the in-shuttle and atom probe vacuum sides) minimized the ingress of contaminants during transfer. The cold chain was maintained through to the “buffer” chamber of the atom probe, and the sample transferred into the cooled “analysis” position. As typical of an atom probe experiment, all data was subsequently acquired at cryogenic conditions.

Data reconstruction and visualization was conducted using IVAS 3.6.6. For this work, overlaps within the mass spectra were not considered to alter any reported results.

Supplementary Figures

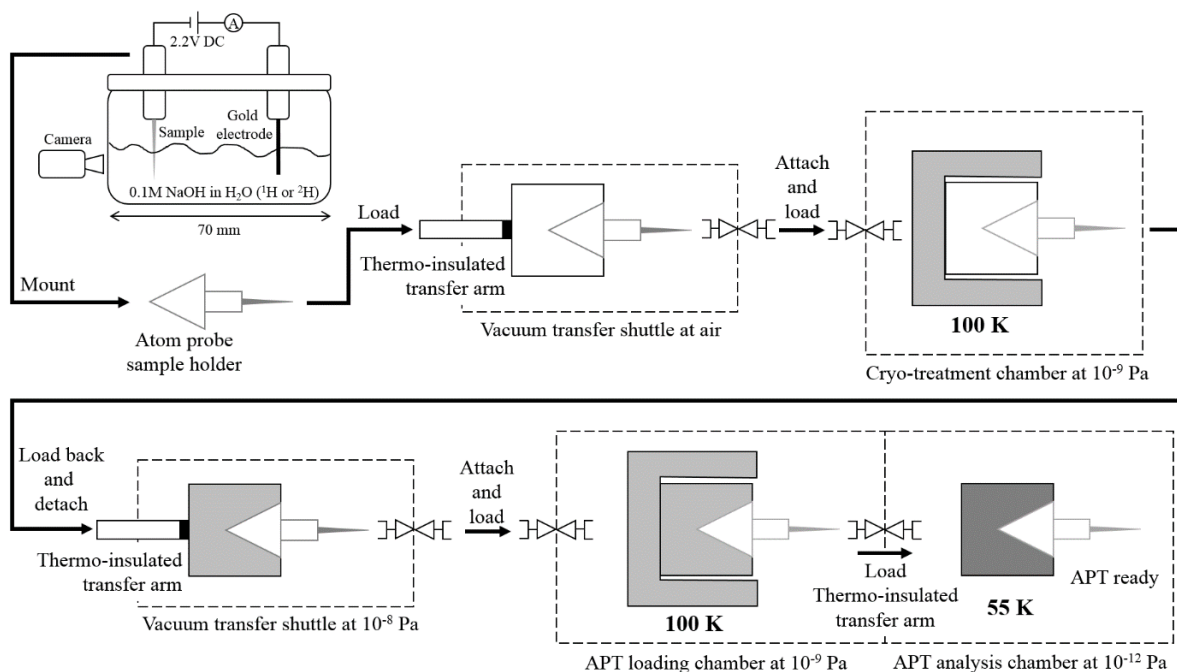


Figure S 1: **Cryogenic transfer protocol.** Schematic of hydrogen charging cell, cooling and subsequent atom probe transfer procedure. The procedure ensures that the sample is cooled as quickly as possible, whilst eliminating contamination (*e.g.* ice formation) from the environment.

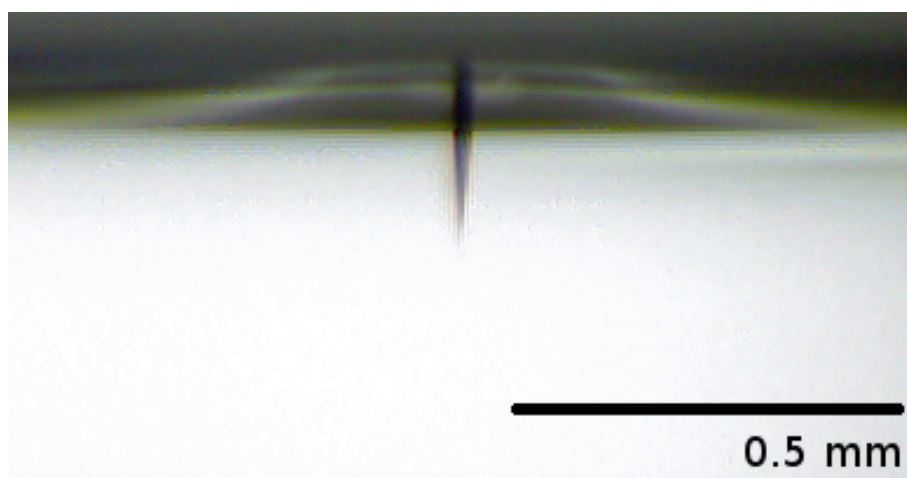


Figure S 2: **Atom probe sample prior to charging.** Camera view of specimen immersed in D_2O solution, immediately after charging completion. Upon application of current, bubbles are observed.

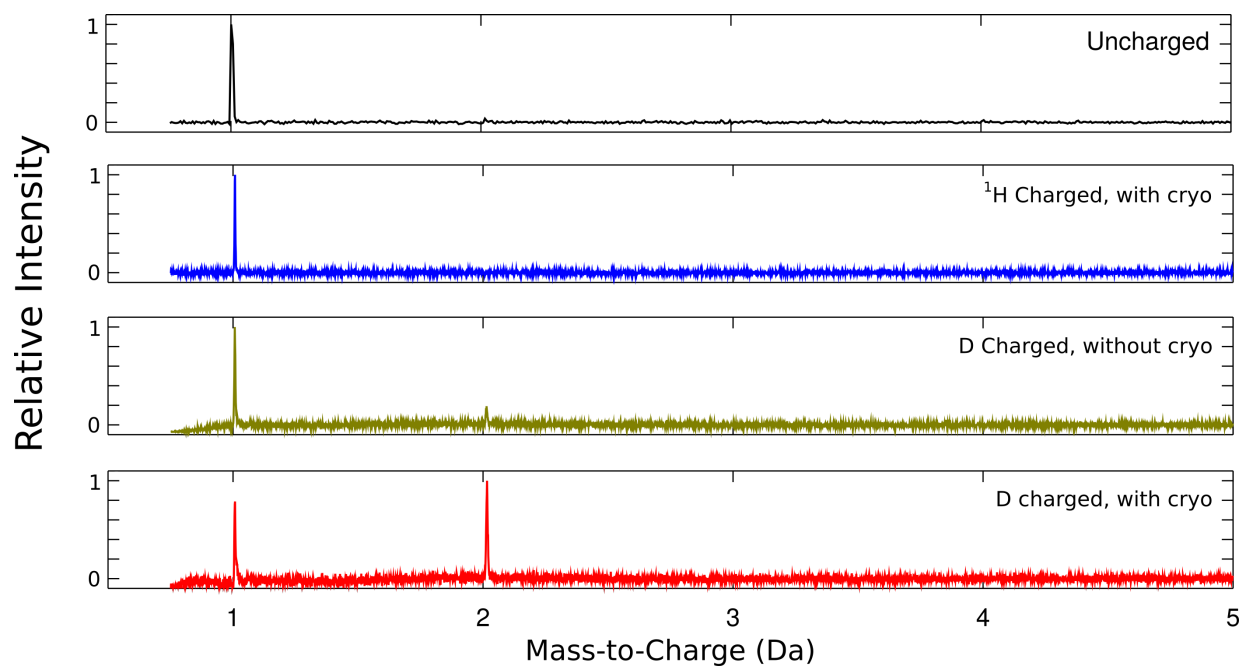


Figure S 3: **Confirmation of isotopic doping efficacy.** Comparison of uncharged, light water charged, and heavy water charged samples. This indicates that no $^1\text{H}_2$ formation has occurred during the analysis. Additionally, for the deuterated sample, 44% of hydrogen (1 or 2) hits were detected as ^1H which is almost certainly artefact, as ^1H (protium) concentrations should not be comparable to that of ^2H (deuterium). Uncharged data acquired on a LEAP 3000 HR system, and charged datasets on the cryo-equipped LEAP4000-XHR system.